Materials Horizons

Unveiling re-entrant phase behavior and crystalline-amorphous interactions in semi-conducting polymer:small molecule blends

Journal:	*Materials Horizons*
Manuscript ID	MH-COM-01-2023-000034.R1
Article Type:	Communication
Date Submitted by the Author:	04-Apr-2023
Complete List of Authors:	Peng, Zhengxing; North Carolina State University, Ade, Harald; North Carolina State University, Department of Physics

Unveiling re-entrant phase behavior and crystalline-amorphous interactions in semi-conducting polymer:small molecule blends

*Zhengxing Peng, Harald Ade**

Department of Physics and Organic and Carbon Electronics Laboratories (ORaCEL), North Carolina State University, Raleigh, North Carolina 27695, United States

* E-mail: hwade@ncsu.edu

New Concepts

We combine two measurement methods previously used in isolation to delineate the phase behavior of blends consisting of complex semi-conducting donor polymer and small molecule acceptors. These measurements delineate unambiguously re-entrant phase behavior for three representative systems, demonstrating unique and complex thermodynamic properties in semi-conducting polymer:small molecule blends. Furthermore, we discover and propose a new approach to measure the crystalline-amorphous interaction parameter χ_{ca}. Our method enables to measure $\chi_{ca}(T)$ over an extended temperature range and not just $\chi_{ca}(T_m)$ near the melting temperature T_m. Such an analysis will pave the way for more extensive studies and better understanding of χ_{ca} in general, but particularly for all the novel non-fullerene acceptors that are able to crystallize.

Abstract

It has been reported recently that conjugated polymer:small molecule systems might exhibit complex, re-entrant phase behavior with hourglass or closed-loop miscibility gaps due to an 'apparent' lower critical solution temperature branch. However, the study did not firmly establish if the observations were reflecting equilibrium or not. To assure that the observed shapes of the binodals via a mixing experiment represent local near-equilibrium conditions that capture complex molecular interactions or equation-of-state effects, we present here the liquidus and the binodal for the exact same systems, *i.e.*, PTB7-Th:$PC_{61}BM$, PffBT4T-C9C13:$PC_{71}BM$ and PTB7-Th:EH-IDTBR, with the liquidus measured via a demixing experiment with long annealing time of days to weeks. We observe that the binodal displayed consistent trends with the liquidus, revealing an underlying thermodynamic and not microstructural or kinetic cause behind the complex phase behavior. Our results highlight the need for a novel, sufficiently complex physical model for understanding these non-trivial phase diagrams of semi-conducting materials. We also discover

that the composition difference ($\Delta\phi$) between liquidus and binodal reflects the crystalline-amorphous interaction, exhibiting a linear relationship with the binodal composition ($\phi_{b,polymer}$), *i.e.*, $\Delta\phi$ increases as χ_{aa} decreases. This possibly provides a new approach for obtaining the crystalline-amorphous interaction parameter $\chi_{ca}(T)$ beyond the commonly used melting point depression method, which estimates χ_{ca} near the melting temperature T_m of the crystalline component. The capability of obtaining $\chi_{ca}(T)$ over a more extended temperature range may encourage more extensive studies and facilitate the understanding of χ_{ca} in general, but particularly for all the novel non-fullerene acceptors that are able to crystallize.

Introduction

Although organic solar cells (OSCs) are now approaching commercially viable efficiencies ($>$ 19%[1-3]), the long-term stability is still a major concern mainly caused by extrinsic degradation with exposure to water and oxygen, intrinsic degradation in the dark, and intrinsic photo-induced degradation[4]. Among them, one important mechanism behind the intrinsic degradation in the dark is ascribed to the reorganization and diffusion of molecules during storage or operation, causing, for example, further phase separation away from the optimal morphology[5] with increased charge recombination and even device shorting[6]. These rearrangements are induced by a thermodynamic driving force for further phase segregation since the solution-cast film is kinetically trapped away from their local and global equilibrium,[7] which are characterized by the temperature-composition ($T-\phi$) phase diagrams[8-12]. The relevance of phase behavior for organic devices and OSCs in particular has been recently reviewed in tutorial fashion.[7] In cases where the blend contains crystallizable component(s), *binodal* and *liquidus* are two important phase boundaries for amorphous-amorphous and crystalline-amorphous interactions in the $T-\phi$ phase diagram, respectively. For a partially miscible blend, such as OPV binaries, a binodal curve (or 'binodal') subdivides the $T-\phi$ space into a single-phase region and a region where two phases coexist, also known as the coexistence region or miscibility gap. When exceeding a critical temperature (T_c), the two components become totally miscible for all compositions, reaching the single-phase region, which renders the so-called upper critical solution temperature (UCST) where the miscibility is increased at higher temperatures.[8] In contrast, lower critical solution temperature (LCST) systems are miscible below T_c for all compositions. A classical statistical model for understanding the binodal is Flory-Huggins (FH) theory[8], with the assumption of incompressibility, based on two main contributors to the free energy of mixing: i) the combinatorial entropy based on the total number of possible microstates and ii) the net enthalpic interaction strength between the individual components. FH theory is a simple and accessible predictive model for UCST with the amorphous-amorphous FH interaction parameter χ_{aa} quantitatively describing the net enthalpic interactions that control the binary miscibility, *i.e.*, larger χ_{aa} corresponds to lower miscibility. Specifically, $\chi(T) \propto (\varepsilon_{pp} + \varepsilon_{ss} - 2\,\varepsilon_{ps}) / kT$, where ε is pairwise enthalpic binding energy between two constituent component where subscripts pp, ps, and ss correspond to polymer-polymer, polymer-SMA, and SMA-SMA interactions. FH theory is intrinsically not capable of describing LCST, which is generally ascribed to strongly directional forces involved,[13] such as hydrogen bonding in mixtures of highly polar species, or complex volume effect with unfavorable equation-of-state contribution[14, 15], leading to demixing driven by entropic effects at higher temperatures. LCST phase behavior can be nonetheless

phenomenologically captured through the use of fitting parameters for χ_{aa}. The liquidus is another important phase boundary for OPV binaries affecting casting kinetics, morphology formation and device stability especially when the small molecule acceptor (SMA) is able to crystallize. The liquidus delineates the miscibility of binary components in the presence of crystals, describing the crystalline-amorphous interactions.

Binodals can be measured with small-angle X-ray/neutron scattering/reflectivity[16, 17] or time-of-flight secondary ion mass spectrometry (ToF-SIMS)[5, 18-21]. Particularly, a few polymer:SMA blends have been reported with a binodal of UCST via bilayer interdiffusion experiment with the help of ToF-SIMS, such as P3HT:$PC_{61}BM$[18, 22], PCDTBT:$PC_{71}BM$[19], P3HT:EH-IDTBR[5], *etc*. In the bilayer interdiffusion experiment, the bilayer is initially composed of a neat polymer layer on the top of a neat SMA layer. At elevated temperature (*i.e.*, thermal annealing), the SMA diffuses into the polymer layer until the volume fraction of SMA in the polymer layer reaches the equilibrium composition, characterized by the binodal, which can be quantified by the depth profile of ToF-SIMS.[5, 19, 20] When the small molecule in polymer:SMA blends is crystallizable, the liquidus can be obtained with scanning transmission X-ray microscopy (STXM)[23-25] or an alternative UV-vis method[26] by extensively annealing the polymer:small molecule blend thin films until micrometer-scale crystals are formed. Recently, it has been reported[20] that the binodal measured from ToF-SIMS for a few polymer:SMA systems might exhibit complex re-entrant phase diagrams, *i.e.*, consisting of an UCST and an 'apparent' LCST branch, resulting in a shape of hourglass or closed-loop. The underlying physical causes of this complexity are still elusive. Additionally, a weakness of the original study is the question of whether the 'apparent' LCST phase behavior is in part the result of an artifact because the polymer layers utilized was quenched to a non-equilibrium state during spin coating, a state that might relax to different degrees at the elevated temperatures used for the interdiffusion experiments.

In order to assure definitively that the observed complex phase diagrams represent near-equilibrium conditions and are indeed the result of thermodynamic and not kinetic factors, we measure the binodal via ToF-SIMS[20] and the liquidus with a UV-vis method[26] for three representative systems: two polymer:fullerene systems, *i.e.*, PTB7-Th:$PC_{61}BM$ and PffBT4T-C9C13:$PC_{71}BM$, and one polymer:nonfullerene system, *i.e.*, PTB7-Th:EH-IDTBR. For measurements performed to determine the binodal, the bilayer films are post-annealed as short as possible to avoid any possible aggregates or crystallization of the small molecule since binodal characterizes the amorphous-amorphous interactions, yet allow for small molecule diffusing into the polymer layer (matrix)[20] for mixing. In contrast, in the liquidus measurements, to make sure the small molecules are crystallized sufficiently, the blend films are post annealed for days, even weeks, so that the small molecules in excess of the equilibrium concentration diffuse out of the polymer matrix and create large, thick crystals[26]. In this case, the relaxation of the components and thus a change in free volume or molecular stacking, *i.e.*, any kinetic or micro-structural effects, cannot be the causative factor for observing an hourglass or closed-loop phase boundary. We observe that the binodals and liquidus are in good agreement with each other, *i.e.*, both the binodals and liquidus exhibit closed-loop phase diagram for PffBT4T-C9C13:$PC_{71}BM$ and PTB7-Th:$PC_{61}BM$ and hourglass phase diagram for PTB7-Th:EH-IDTBR. Moreover, we study a binodal control system, PTB7-Th:di-PDI, where the small molecule cannot crystalize and we pre-anneal

the polymer thin films at different temperatures before making bilayers for the interdiffusion experiments, relaxing polymer chains to exclude any possible kinetically quenched states created during spin casting. As a result, the measured trend of the miscibility remains unchanged with only a subtle shift in composition at high temperatures. The control studies and the observed similarities between the binodal and liquidus demonstrate that the complex hourglass or closed-loop phase diagrams indeed represent thermodynamic equilibrium states, and there are intrinsic fundamental thermodynamic causes for the complex phase diagrams.

Furthermore, the composition difference between binodal and liquidus ($\Delta\phi$) is related to difference in the chemical potential between the crystals and their liquid state (*i.e.*, amorphous state[7]), as well the interactions of amorphous mixed phase and small molecule crystal phase. We noticed that $\Delta\phi$ exhibits an almost linear relationship with the binodal composition ($\phi_{b,polymer}$). With assuming the crystalline-amorphous interaction parameter $\chi_{ca}(T)$ is proportional to 1/T, we can estimate $\chi_{ca}(T)$, which is indeed a new method to determine such crystalline-amorphous interactions beyond the conventional melting point depression approach.

Results and discussion

We utilized primarily polymer:fullerene systems since PCBM tends to form micrometer-sized crystals easily at low temperature and such systems are amenable to using the UV-vis method[26] to determine the liquidus. The two representative polymers used are PTB7-Th and PffBT4T-C9C13. Although a recent study indicates PTB7-Th is semi-paracrystalline[27], it is highly disordered with a paracrystalline *g* parameter of ~18%[28], which is higher than g = 12% that generally marks the boundary of amorphous and para-crystalline. PffBT4T-C9C13 represents polymers with temperature dependent aggregation in solution[29] that exhibit clear melting (T_m ~ 261.9 ℃, **Figure S1**) in conventional differential scanning calorimetry (DSC) and a paracrystalline *g* parameter (11%) that is lower than 12%[28]. These two polymers represent thus materials with rather different molecular packing. We also studied a polymer:nonfullerene system, PTB7-Th:EH-IDTBR, as complement to have some small molecule diversity. The binodals are measured following the reported bilayer interdiffusion protocol[20]. The bilayer films are made with water-floating method where polymer thin films are spun-cast onto polystyrene sulfonate (PSS) coated substrates and then floated on a water surface to be picked up by a Si-supported small-molecule film. The dried bilayer films are post annealed at different temperatures to allow the small molecules to diffuse into the polymer layer. The equilibrium miscibility is measured or estimated with ToF-SIMS. The annealing time ranged from seconds to hours, for temperature above and below small molecule glass transition temperature T_g, respectively. The ToF-SIMS profiles for PTB7-Th:$PC_{61}BM$ are reported in ref[20] while SIMS profiles for PffBT4T-C9C13:$PC_{71}BM$ and PTB7-Th:EH-IDTBR are shown in **Figure S3**. The liquidus is measured with a UV-vis method[26] where the spun-cast blend thin films with an initial high volume fraction of small molecules are post annealed at different temperatures so that PCBM or EH-IDTBR in excess of the liquidus composition will be driven to diffuse out of the mixed phases to form large crystals readily detectable with optical microscopy (see **Figure 1**). When the crystal formation forces the matrix composition to reach the local thermodynamic equilibrium, the composition in the amorphous mixed phases equals the liquidus

composition. Due to absorption saturation, the thick crystals do not contribute much to the observed spectra and the liquidus can be determined with fitting the UV-vis spectra with linear combinations of reference spectra[26]. The typical annealing time is three to four days, or even weeks for slowly evolving systems, *e.g.*, EH-IDTBR at low temperatures.

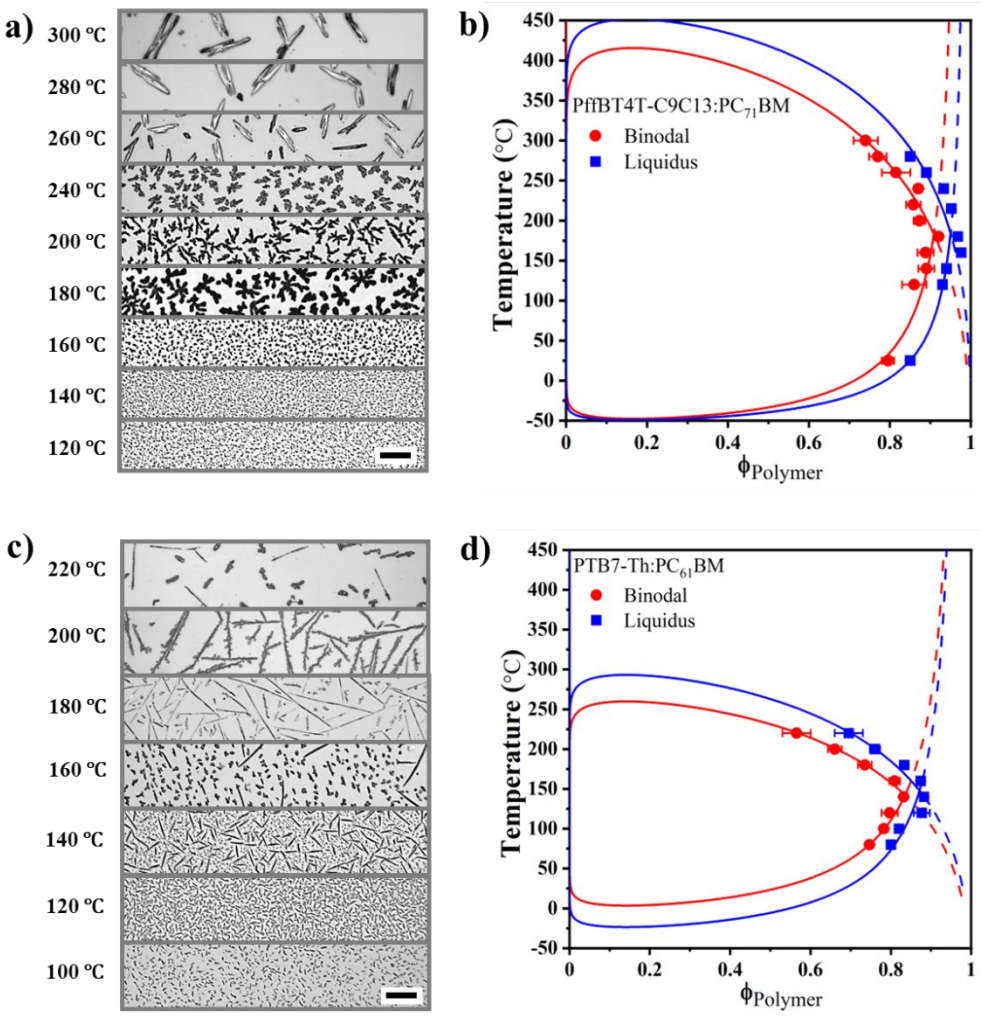

Figure 1. a) Transmission optical micrographs of 60:40 (wt%) PTB7-Th:$PC_{61}BM$ thin films deposited on glass substrates annealed at 100 °C to 220 °C for three to four days. b) $T-\phi$ phase diagram with binodal from ToF-SIMS and liquidus from UV-vis method for PTB7-Th:$PC_{61}BM$. c) Transmission optical micrographs of 50:50 (wt%) PffBT4T-C9C13:$PC_{71}BM$ thin films deposited on glass substrates annealed at 120 °C to 300 °C for three to four days. b) $T-\phi$ phase diagram with binodal and liquidus for PffBT4T-C9C13:$PC_{71}BM$. The scale bars in a) and c) represent 50 μm. The error bars are derived from different experimental runs. The solid lines in b) and d) represent separate UCST or LCST fits to subsets of the data using Flory-Huggins (FH) theory with fitted parameters shown in **Table S1**. They are extrapolated to the outside of the fitting range and used as guides to the eyes to better see the closed loop phase-diagram characteristics.

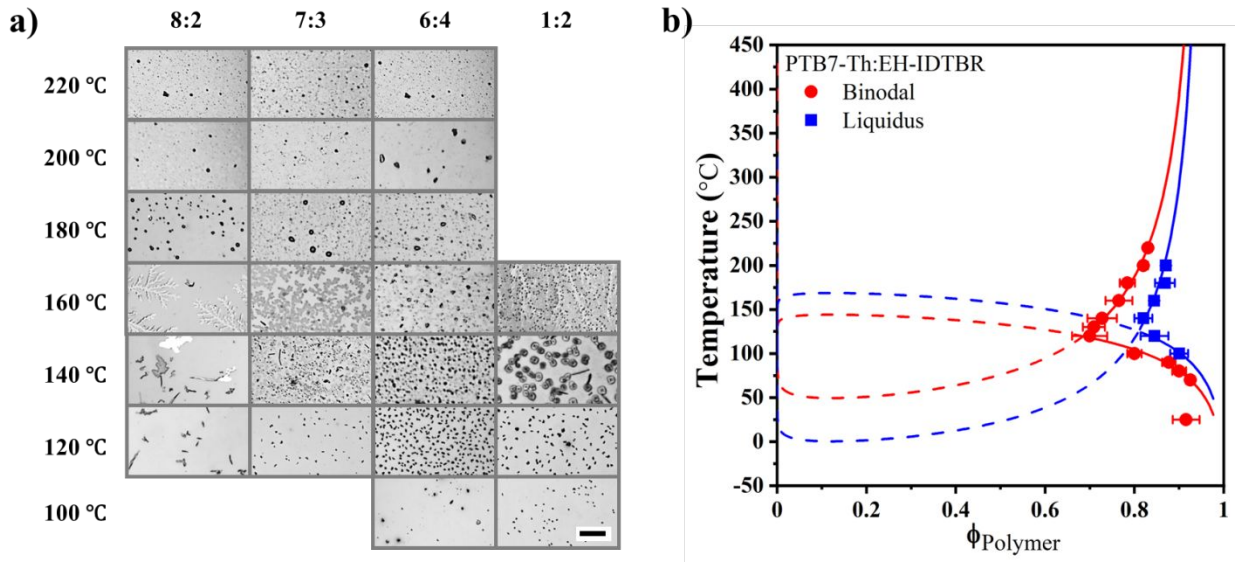

Figure 2. a) Transmission optical micrographs of PTB7-Th:EH-IDTBR thin films with different D/A ratios deposited on glass substrates annealed at 100 °C to 200 °C for two to four weeks. The scale bar represents 50 μm. b) $T - \phi$ phase diagram with binodal and liquidus. The error bars are from different experimental runs. The solid lines represent separate UCST or LCST fits to subsets of the data using Flory-Huggins theory with fitted parameters shown in **Table S1**. They are extrapolated to the outside of the fitting range and used as guides to the eyes to better see the hour-glass phase-diagram characteristics (The left part of the hourglass is not perceptible, as it is too close to $\phi = 0$). Dashed lines help appreciate the segmented FH behavior.

The measured liquidus (**Figure 1**) exhibit closed-loop phase behavior for PTB7-Th:$PC_{61}BM$ and PffBT4T-C9C13:$PC_{71}BM$, with binodal a similar trend. In PTB7-Th:$PC_{61}BM$, the miscibility (volume fraction of polymer) decreases from 20% (liquidus) and 25% (binodal) small molecules at 80 ℃ to 12% (liquidus) and 17% (binodal) small molecules at 140 ℃, *i.e.*, the low-T branch is LCST, and then increases to 30% (liquidus) and 43.5% (binodal) small molecules at 220 ℃, *i.e.*, the high-T branch is UCST. For PffBT4T-C9C13:$PC_{71}BM$, the miscibility decreases from 15% (liquidus) and 20.5% (binodal) at 25 ℃ to 3.2% (liquidus) and 8% (binodal) small molecules at 180 ℃, *i.e.*, the LCST branch, and then increases to 15% (liquidus) and 23% (binodal) small molecules at 280 ℃, *i.e.*, the UCST branch. Both the liquidus and binodal of PTB7-Th:EH-IDTBR exhibit an hourglass phase diagram: the miscibility increases from 10% (liquidus) at 100 ℃ to 18% (liquidus) small molecules at 140 ℃ and from 8% (binodal) at 25 ℃ to 32% (binodal) small molecules at 120 ℃, *i.e.*, the low-T branch is UCST, and then decreases to 13% (liquidus) and 18% (binodal) small molecules at 200 ℃, *i.e.*, the high-T branch is LCST. The binodal follows the outlines of the liquidus closely with a similar transition temperature between the UCST and LCST behavior. In all cases is the liquidus to the right of the binodal, *i.e.*, the part in the phase diagram that corresponds to smaller concentrations of the small molecule in the polymer phase. This is consistent with the presence of an extra chemical potential of the small molecule crystal and

repulsive amorphous-crystal interactions that deplete the concentration of the small molecule below the binodal concentration.

The bilayer experiment approaches the binodal from the unmixed state (the right side in the phase diagram) while the UV-vis experiment approaches the liquidus from the mixed state (the left side of the phase diagram). Additionally, the annealing time is very different and kinetic effects that might impact the measurements need to be considered. The common understanding of small molecule diffusion into or out of a polymer matrix assumes that different sized microcavities, *i.e.*, free volume, are continuously formed and destroyed in the polymer matrix as a result of random motions of polymer segments induced by thermal energy fluctuations[30]. Small molecules can 'jump' to the microcavities with suitable size by 'random walk' when they occasionally acquire sufficient thermal energy. The driving force is the gradient of concentration or chemical potential. A true thermodynamic equilibrium means there is no composition gradient in any phase. To reach it via mixing or demixing, it requires uniform films and sufficient diffusion distance/time. In an actual experiment, the true thermodynamic equilibrium is hardly achieved since there are always defects or the mixing/demixing process is slowed down when the driving force is decreased as it is close to the equilibrium, or the kinetics is slowed down due to the slowing down fluctuations at low temperatures. However, the observed consistence and correspondence between the binodal from mixing and the liquidus from demixing suggests that the possible effects away from ideal cases is small enough to be neglected and the observed results indeed represent local near-equilibrium conditions of the disordered polymer volume fraction and the observed complex phase diagrams have an intrinsic thermodynamics cause.

Regarding our observations in relation to thermodynamic equilibrium, we specifically note that PffBT4T-C9C13:$PC_{71}BM$ is expected and confirmed by DSC (see **Figure S2**) to be a eutectic system[6] as both materials can crystallize. At equilibrium, there are only two crystalline phases below the eutectic temperature with the solvus reflecting the phase. This is not the case in our measurements and reflects the fact that polymers never reach equilibrium and even highly crystalline polymers have a large volume fraction of a disordered phase during typical experimental time scales. Our measurements are targeting the interactions of this disordered phase and yield the meta-stable binodal if the small molecule remains disordered. Similarly, the liquidus determined here corresponds to the metastable, local equilibrium of the disordered polymer phase with the small molecule crystals. The polymer para-crystals in the thin films are quasi non-interacting 'bystanders' who are kinetically frozen out and unable to deplete the mixed domains of polymer segments and increase the degree of crystallinity within the time scales of the measurements.

An experimental way to assess possible kinetic or micro-structural effects and changes in the degree of polymer ordering in the binodal measurements is to pre-anneal the polymer layers before making the bilayers for interdiffusion experiments. The pre-annealing can not only relax polymer chains to release the conformational freedom, *i.e.*, structural recovery via physical aging, but remove possible defects and inhomogeneity, which are possible kinetic factors that might affect sufficient mixing. We utilized PTB7-Th:di-PDI for this purpose since it has shown an hourglass phase behavior previously[20] and both components are highly disordered with minimal micro-

structural changes upon annealing. PTB7-Th:di-PDI is an excellent candidate for binodal measurements. PTB7-Th exhibits a broad thermal relaxation at ~ 113 ℃ with dynamic mechanical analysis (DMA)[31] that may or may not be a T_g, while di-PDI exhibit a clear T_g at ~ 137 ℃ without any melting in DSC measurement (**Figure S1**). di-PDI does not show strong molecular packing in X-ray scattering with only diffuse halos.[20] Longer annealing is thus possible with di-PDI than with crystallizable small molecules. The PTB7-T-h layers are pre-annealed at different temperatures to allow sufficient structural recovery. Results are displayed in **Figure 3**. No matter what temperature the polymer thin films are pre-annealed at, below or above T_g, the overall hourglass shape of the binodal remains unchanged, indicating that kinetic effects such as structural relaxation of PTB7-Th cannot be the causative factors for the observed complex, re-entrant phase diagrams.

Even though we observe consistent overall shape of the binodal using films that were pre-annealed, there are subtle systematic shifts of the binodal at temperatures above the 'kink' temperature with pre-annealing conditions. PTB7-Th is reported as semi-paracrystallline.[27] If the subtle shift is due to the increased degree of para-crystallinity with increased pre-annealing temperature and smaller volume fraction of disordered materials, the measured miscibility would need to be corrected for this degree of para-crystallinity. Such an increase in polymer ordering would shift the measured binodal to the right as the volume fraction of material in which the small molecule can be dissolved in has decreased. However, the results exhibit the opposite trend and must therefore arise from a different cause and mechanism such as changes primarily related to effects arising from the disordered volume-fraction. FH theory assumes the incompressibility of systems and gives χ_{aa} in the form of: $\chi_{aa} = A + \frac{B}{T}$, where A is the entropic term, B/T is the enthalpic term. However, the LCST branch in the hourglass shaped phase diagram suggests that the free volume effects cannot be neglected here. Considering the compressibility, the FH interaction parameter can be written in the form of:[32] $\chi_{aa} = A + \frac{B}{T} + ClnT$, with $ClnT$ term added to account for the effect of the free volume changes with temperature. We follow arguments in our prior publication[20] to fit the experimental binodal data with the above form as a function of pre-annealed condition. As a result, the fitted C is decreasing with pre-annealing temperature (**Figure S6**), suggesting that the free volume effects decrease with increased pre-annealing temperature. This would constitute a residual kinetic effect. We note that a free volume decrease is consistent with an increase of the degree of ordering, but the effects on the binodal are different from geometric volume effects and our observations are driven by thermodynamic factors.

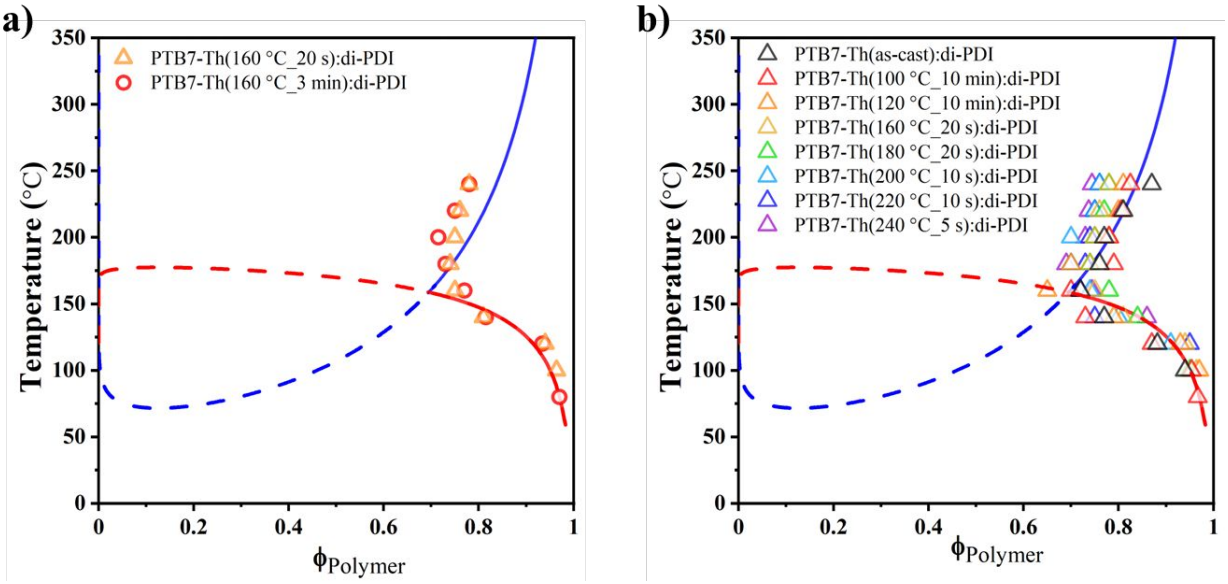

Figure 3. a) Comparison between the phase diagram from pre-annealing PTB7-Th layers at 160 ℃ for different time. The consistency suggests that 20 s pre-annealing is enough for structural recovery at 160 ℃. b) $T-\phi$ phase diagram for PTB7-Th:di-PDI with PTB7-Th thin film pre-annealed at different temperatures before making bilayers to allow polymer chains relax. The dashed/solid lines represent the UCST or LCST Flory-Huggins fits for as-cast films as guides to the eye.

Although the liquidus and binodal in **Figures 1** and **2** demonstrate similar shape of the phase boundaries, the composition difference between the liquidus and binodal ($\Delta\phi = \phi_{l,polymer} - \phi_{b,polymer}$) is not constant, as shown in **Figure 4a**, and shows divergent trends as a function of system and temperature. For PffBT4T-C9C13:$PC_{71}BM$, $\Delta\phi$ is small at low temperatures, and then increases almost linearly with temperature above T_g of $PC_{71}BM$ (~163 ℃ from **Figure S1**). For two PTB7-Th systems, $\Delta\phi$ is increasing with temperature for PTB7-Th:$PC_{61}BM$ but decreasing for PTB7-Th:EH-IDTBR. We interpret the divergence between the two PTB7-Th systems to imply that the difference cannot be due to the observed changes in free volume discussed above but must be due to specific intermolecular interactions with the crystals now present for the liquidus relative to the amorphous interaction that are encoding the binodal ϕ_b and its shape. We note that these two PTB7-Th blends have hourglass and closed-loop shape, respectively, and if the data is examined as $\Delta\phi$ versus $1-\phi_{b,polymer} = \phi_{b,SMA}$ as shown in **Figure 4b**, the divergence is resolved and all systems show a similar, possibly linear trend. $\Delta\phi$ increases as χ decreases.

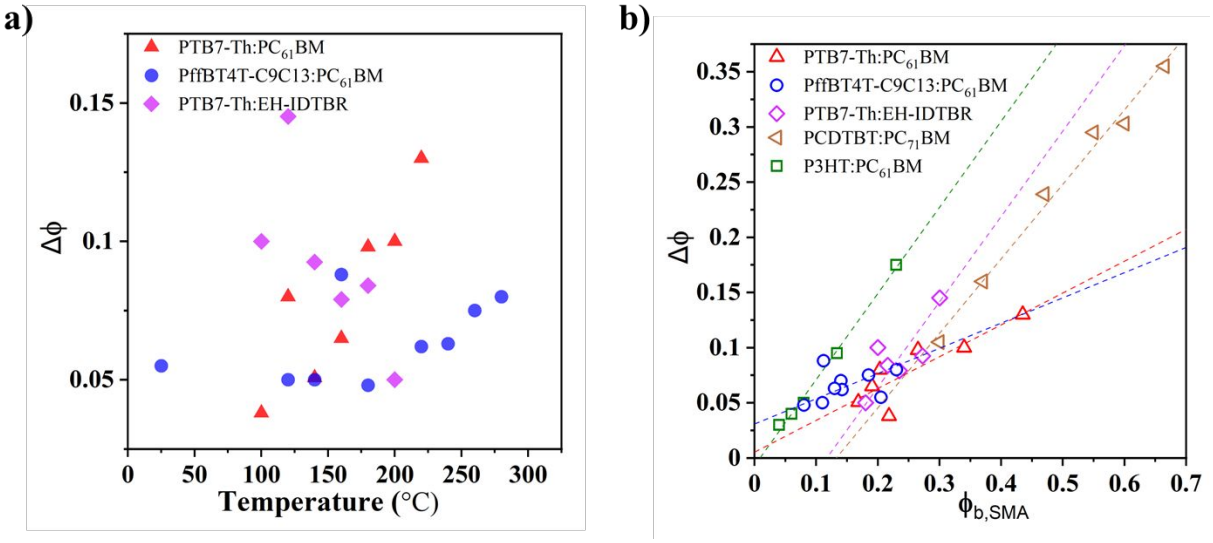

Figure 4. a) The composition difference between liquidus and binodal at different temperatures. b) $\Delta\phi$ *vs.* $1-\phi_{b,polymer}$ plot. We utilize $\phi_{b,SMA}$ rather than $\phi_{l,SMA}$ as the ordinate because our reference frame is the binodal and their segmented fits for UCST and LCST behavior, respectively.

In order to guide our discussion and further analysis, we utilize previously published differences between the binodal and the liquidus for PCDTBT:$PC_{71}BM$[10, 19] and P3HT:$PC_{61}BM$[18, 22], purely UCST systems based on one amorphous polymer and one semi-paracrystalline polymer for which large differences in $\Delta\phi$ have been observed (reproduced at **Figure S7**). The different phase behaviors of UCST in PCDTBT:$PC_{71}BM$ and P3HT:$PC_{61}BM$ versus the re-entrant phase diagrams reported here lies on the dissimilarity in cohesive energy density and chemical dissimilarity of the binary components, compressibility and thermal expansion coefficients. Better understanding will rely on a further development of a novel, sufficiently complex physical model beyond FH theory that will have to capture the underlying, as yet unknown, parameters. The re-entrant phase behavior is likely a result of various free energy contributions, including three enthalpic contributions (inter- and intra-molecular contributions and a contribution due to expansion work) and three entropic contributions (combinatorial, equation-of-state and configurational contributions) in a complicated way.

When represented as $\Delta\phi$ versus $1-\phi_{b,polymer}$ in **Figure 4b**, the PCDTBT:$PC_{71}BM$ data clearly suggest a linear relation between $\Delta\phi$ and $1-\phi_{b,polymer}$. Unfortunately, there is no analytical expression for such a possible relation. Both the binodal and liquidus are determined computationally via a common tangent method of the Gibbs free energy with composition. The binodal is derived from original FH with $\chi_{aa} = A + \frac{B}{T}$. For the liquidus, solidus and solvus, the free energy that takes crystalline-amorphous interactions into account has been expressed by Kyu et al.[33, 34] as:

$$f(\psi,\phi) = f_{mixing} + \phi f_{crystal} + f_{crystalline-amorphous\ interaction}$$
$$= \frac{\phi}{r_1}\ln(\phi) + \frac{1-\phi}{r_2}\ln(1-\phi) + \chi_{aa}\phi(1-\phi) + \phi f(\psi) + \chi_{ca}[\phi\psi][(1-\phi)\psi] \quad (1)$$

Where ϕ and $(1-\phi)$ are volume fractions of the crystalline and amorphous components, r_1 and r_2 are the degree of polymerization, ψ is the crystal phase order parameter defined as the ratio of lamellar thickness to that of a perfect crystal. The first three terms in equation (1) are the terms of the FH equation that do not depend on ψ. χ_{ca} is assumed to be proportional to $\Delta H/RT$,[34] similar to the $1/T$ dependence of the original FH for χ_{aa}. Whether or not such an ideal behavior is exhibited by real systems is unclear. With the assumption that $\chi_{ca} \propto 1/T$ and that ψ does not materially change over the temperature range of our analysis, we fitted the liquidus with two separate branches with $\chi_L = A + \frac{B}{T}$. Keeping A fixed from the binodal fits works for the two PTB7-Th systems but not for the PffBT4T-C9C13 system (see Supporting Information **Table S1**). Assuming that $\psi \sim 1$ and comparing the fits, we estimate $\chi_{ca} = 60/T$ for the low-T branch and $\chi_{ca} = 87/T$ for the high-T branch for PTB7-Th:$PC_{61}BM$, $\chi_{ca} = 151/T$ and $\chi_{ca} = 105/T$, respectively, for PTB7-Th:EH-IDTBR, while $\chi_{ca} = 1.25 - 312/T$ and $\chi_{ca} = -0.52 + 453/T$, respectively, for PffBT4T-C9C13:$PC_{71}BM$. Given that we observe differences in χ_{ca} below and above T_g for all three systems, although to varying degree, suggests that the glass transition has an impact on χ_{ca} similar to the impact it has on χ_{aa}.

Crystalline-amorphous interactions are also an important factor in determining device stability. The morphological evolution during the intrinsic degradation in the dark is induced by two major factor: i) further phase separation via demixing driven by amorphous-amorphous interactions, *e.g.*, binodal and ii) crystallization failure due to the nucleation and growth of SMA crystals characterized by crystalline-amorphous interactions (liquidus)[5]. Large χ_{ca} suggests a repulsive interaction between the crystalline and amorphous phases, which will facilitate the formation of pure crystalline phases, *i.e.*, crystals. The linearity observed in **Figure 4b** suggests a monotonic, possibly algebraic relations between χ_{ca} and χ_{aa}, that holds above and below the T_g. In this case, device stability will be mediated by the trade-off between χ_{ca} and χ_{aa}. A dependence of χ_{ca} on free volume and or directional forces similar to the factors that drive the LCST behavior of χ_{aa} is readily conceivable. Only detailed analysis of the differences between the liquidus and binodal involving computational comparisons and possibly improved modeling and more extensive data sets would allow such an assessment in detail.

We note that our analysis provides a potentially new approach to measure χ_{ca} beyond the commonly used one, *i.e.*, the melting point depression.[34-36]. It has been generally recognized[36] that χ_{ca} obtained from melting point depression is underestimated in most cases since the experimentally determined melting points from DSC hardly represent the equilibrium conditions. If crystallization has, for instance, taken place under fast supercooling, a reduced crystal size can suppress the melting point due to the Gibbs-Thompson effect[37], which will be entangled with the 'thermodynamic' depression. However, an analysis that utilizes the differences between the liquidus and binodal avoids these issues since the extensive annealing preceding the liquidus

measurements reaches the near-equilibrium state and the obtained liquidus composition is independent of crystallization mechanism and kinetics[26]. Furthermore, such an analysis would be able to measure $\chi_{ca}(T)$ over an extended temperature range and not just $\chi_{ca}(T_m)$ near the melting temperature T_m.

Conclusions

In summary, this work compares the binodal from a mixing experiment with the liquidus from a long-time demixing experiment for three representative polymer:small molecule systems. Both binodal and liquidus exhibit the similar re-entrant phase diagrams, hourglass or closed-loop. This demonstrates that the observed complex phase diagrams indeed have a thermodynamic cause and are not resulting from microstructural artifacts arising during sample-preparation or measurements. As a further confirmation and to exclude detrimental kinetic effects in interdiffusion experiments, we pre-annealed the polymer layer for structural relaxation, and no substantial difference was observed except slight shift in miscibility values at high temperatures, indicative of decreasing free volume effects. Our data highlights the intrinsic underlying thermodynamics behind the non-trivial, re-entrant phase behaviors in conjugated polymer:small molecule systems, which will need further studies and a novel, sufficiently comprehensive physical model for complete understanding. We also delineate a potential methodology for obtaining $\chi_{ca}(T)$ experimentally beyond the commonly used melting point depression method that measures $\chi_{ca}(T_m)$ near melting temperature. The capability of obtaining $\chi_{ca}(T)$ over an extended temperature range may encourage more studies beyond semi-conducting materials and facilitate in particular the understanding of χ_{ca} given that the high-performing small molecule acceptors tend to crystallize and χ_{ca} needs to be explored more extensively.

Associated content

Supporting Information

Experimental methods, Chemical structure, DSC data, ToF-SIMS profiles and UV-vis spectra.

Conflicts of interest

The authors declare no competing interests.

Acknowledgements

The authors would like to acknowledge the support from the ONR grant N000142012155 and general discussions about phase diagrams with Jasper Michels (Max Plank Institute for Polymer Research, Mainz, Germany).

References

1. L. Zhu, M. Zhang, J. Q. Xu, C. Li, J. Yan, G. Q. Zhou, W. K. Zhong, T. Y. Hao, J. L. Song, X. N. Xue, Z. C. Zhou, R. Zeng, H. M. Zhu, C. C. Chen, R. C. I. MacKenzie, Y. C. Zou, J. Nelson, Y. M. Zhang, Y. M. Sun and F. Liu, *Nat. Mater.*, 2022, **21**, 656-663.
2. Y. Cui, Y. Xu, H. F. Yao, P. Q. Bi, L. Hong, J. Q. Zhang, Y. F. Zu, T. Zhang, J. Z. Qin, J. Z. Ren, Z. H. Chen, C. He, X. T. Hao, Z. X. Wei and J. H. Hou, *Adv. Mater.*, 2021, **33**.
3. K. Jiang, J. Zhang, C. Zhong, F. R. Lin, F. Qi, Q. Li, Z. X. Peng, W. Kaminsky, S. H. Jang, J. W. Yu, X. Deng, H. W. Hu, D. Shen, F. Gao, H. Ade, M. Xiao, C. F. Zhang and A. K. Y. Jen, *Nat. Energy*, 2022, **7**, 1076-1086.
4. W. R. Mateker and M. D. McGehee, *Adv. Mater.*, 2017, **29**.
5. M. Ghasemi, H. W. Hu, Z. X. Peng, J. J. Rech, I. Angunawela, J. H. Carpenter, S. J. Stuard, A. Wadsworth, I. McCulloch, W. You and H. Ade, *Joule*, 2019, **3**, 1328-1348.
6. N. Li, J. D. Perea, T. Kassar, M. Richter, T. Heumueller, G. J. Matt, Y. Hou, N. S. Güldal, H. Chen, S. Chen, S. Langner, M. Berlinghof, T. Unruh and C. J. Brabec, *Nat. Commun.*, 2017, **8**, 14541.
7. Z. Peng, N. Stingelin, H. Ade and J. J. Michels, *Nat Rev Mater*, 2023.
8. P. J. Flory, *Principles of Polymer Chemistry*, Cornell University Press, Ithaca, 1953.
9. N. Stingelin, *Polym. Int.*, 2012, **61**, 866-873.
10. L. Ye, B. A. Collins, X. C. Jiao, J. B. Zhao, H. Yan and H. Ade, *Adv. Energy Mater.*, 2018, **8**, 1703058.
11. N. D. Treat, A. Varotto, C. J. Takacs, N. Batara, M. Al-Hashimi, M. J. Heeney, A. J. Heeger, F. Wudl, C. J. Hawker and M. L. Chabinyc, *J. Am. Chem. Soc.*, 2012, **134**, 15869-15879.
12. J. R. Tumbleston, L. Yang, W. You and H. Ade, *Polymer*, 2014, **55**, 4884-4889.
13. T. Ougizawa and T. Inoue, *Polym. J.*, 1986, **18**, 521-527.
14. R. E. Bernstein, C. A. Cruz, D. R. Paul and J. W. Barlow, *Macromolecules*, 1977, **10**, 681-686.
15. S. S. Kim and D. R. Lloyd, *Polymer*, 1992, **33**, 1026-1035.
16. F. A. Bokel, S. Engmann, A. A. Herzing, B. A. Collins, H. W. Ro, D. M. DeLongchamp, L. J. Richter, E. Schaible and A. Hexemer, *Chem. Mater.*, 2017, **29**, 2283-2293.
17. A. M. Higgins, P. Gutfreund, V. Italia and E. L. Hynes, *Journal of Materials Chemistry C*, 2023, **11**, 2107-2119.
18. N. D. Treat, T. E. Mates, C. J. Hawker, E. J. Kramer and M. L. Chabinyc, *Macromolecules*, 2013, **46**, 1002-1007.
19. L. Ye, H. W. Hu, M. Ghasemi, T. H. Wang, B. A. Collins, J. H. Kim, K. Jiang, J. H. Carpenter, H. Li, Z. K. Li, T. McAfee, J. B. Zhao, X. K. Chen, J. L. Y. Lai, T. X. Ma, J. L. Bredas, H. Yan and H. Ade, *Nat. Mater.*, 2018, **17**, 253-260.
20. Z. Peng, N. Balar, M. Ghasemi and H. Ade, *J. Phys. Chem. Lett.*, 2021, **12**, 10845-10853.
21. D. Chen, A. Nakahara, D. Wei, D. Nordlund and T. P. Russell, *Nano Lett.*, 2011, **11**, 561-567.

22. N. D. Treat, M. A. Brady, G. Smith, M. F. Toney, E. J. Kramer, C. J. Hawker and M. L. Chabinyc, *Adv. Energy Mater.*, 2011, **1**, 82-89.
23. B. A. Collins, E. Gann, L. Guignard, X. He, C. R. McNeill and H. Ade, *J. Phys. Chem. Lett.*, 2010, **1**, 3160-3166.
24. B. A. Collins, Z. Li, J. R. Tumbleston, E. Gann, C. R. McNeill and H. Ade, *Adv. Energy Mater.*, 2013, **3**, 65-74.
25. B. A. Collins, J. R. Tumbleston and H. Ade, *J. Phys. Chem. Lett.*, 2011, **2**, 3135-3145.
26. Z. X. Peng, X. C. Jiao, L. Ye, S. S. Li, J. J. Rech, W. You, J. H. Hou and H. Ade, *Chem. Mater.*, 2018, **30**, 3943-3951.
27. S. Marina, E. Gutierrez-Fernandez, J. Gutierrez, M. Gobbi, N. Ramos, E. Solano, J. Rech, W. You, L. Hueso, A. Tercjak, H. Ade and J. Martin, *Mater. Horiz.*, 2022, **9**, 1196-1206.
28. Z. X. Peng, L. Ye and H. Ade, *Mater. Horiz.*, 2022, **9**, 577-606.
29. Y. Liu, J. Zhao, Z. Li, C. Mu, W. Ma, H. Hu, K. Jiang, H. Lin, H. Ade and H. Yan, *Nat. Commun.*, 2014, **5**, 5293.
30. H. L. Frisch and S. A. Stern, *Crit. Rev. Solid State Mater. Sci.*, 2006, **11**, 123-187.
31. N. Balar, S. Siddika, S. Kashani, Z. X. Peng, J. J. Rech, L. Ye, W. You, H. Ade and B. T. O'Conner, *Chem. Mater.*, 2020, **32**, 6540-6549.
32. D. Kim, T. Kyu and T. Hashimoto, *J. Polym. Sci. Pol. Phys.*, 2006, **44**, 3621-3630.
33. R. A. Matkar and T. Kyu, *J. Phys. Chem B*, 2006, **110**, 12728-12732.
34. P. Rathi, T. M. Huang, P. Dayal and T. Kyu, *J. Phys. Chem. B*, 2008, **112**, 6460-6466.
35. T. Nishi and T. T. Wang, *Macromolecules*, 1975, **8**, 909-915.
36. P. B. Rim and J. P. Runt, *Macromolecules*, 1982, **17**, 1520-1526.
37. L. Scalfi, B. Coasne and B. Rotenberg, *J. Chem. Phys.*, 1990, **93**, 9002.